

The First X-Ray Polarimetry of an Eclipsing Low-Mass X-Ray Binary: Serendipitous IXPE Observation of AX J1745.6–2901

ROMANA MIKUŠINCOVÁ ¹, LORENZO MARRA ¹, HEMANTH MANIKANTAN ¹, STEFANO BIANCHI ²,
FIAMMA CAPITANIO ¹, SUDIP CHAKRABORTY ³, RAUL CIANCARELLA ⁴, ENRICO COSTA ¹, NICOLAS DE ANGELIS ¹,
MELANIA DEL SANTO ⁵, SERGIO FABIANI ¹, RICCARDO FERRAZZOLI ¹, VITTORIA E. GIANOLLI ⁶,
ANDREA GNARINI ², ADAM INGRAM ⁷, SHIFRA MANDEL ⁸, GUGLIELMO MASTROSERIO ⁹, GIORGIO MATT ²,
KAYA MORI ⁸, FABIO MULERI ¹, SIMONE PAGLIARELLA ^{1,10,11}, MAXIME PARRA ¹², P.O. PETRUCCI ¹³,
JAKUB PODGORNÝ ¹⁴, JURI POUTANEN ¹⁵, SWATI RAVI ¹⁶, PAOLO SOFFITTA ¹, JAMES F. STEINER ¹⁷,
ANTONELLA TARANA ¹, ROBERTO TAVERNA ¹⁸, FRANCESCO URSINI ², ALEXANDRA VELEDINA ^{15,19},
FEDERICO M. VINCENTELLI ^{1,20}, ANASTASIYA YILMAZ ¹, BARBARA DE MARCO ²¹, MAITRAYEE GUPTA ¹⁴,
VLADISLAV LOKTEV ⁷, THOMAS D. RUSSELL ⁵, JIŘÍ SVOBODA ¹⁴, FRANCESCO TOMBESI ¹⁰ AND SHUO ZHANG ²²

¹INAF Istituto di Astrofisica e Planetologia Spaziali, Via del Fosso del Cavaliere 100, 00133 Roma, Italy

²Dipartimento di Matematica e Fisica, Università degli Studi Roma Tre, Via della Vasca Navale 84, 00146 Roma, Italy

³Science and Technology Institute, Universities Space and Research Association, Huntsville, AL 35805, USA

⁴Independent Researcher

⁵INAF Istituto di Astrofisica Spaziale e Fisica Cosmica, Via U. La Malfa 153, I-90146 Palermo, Italy

⁶Department of Physics and Astronomy, Clemson University, Clemson, SC, 29634, USA

⁷School of Mathematics, Statistics, and Physics, Newcastle University, Newcastle upon Tyne NE1 7RU, UK

⁸Columbia Astrophysics Laboratory, Columbia University, New York, NY 10027, USA

⁹Scuola Universitaria Superiore IUSS Pavia, Palazzo del Broletto, piazza della Vittoria 15, I-27100 Pavia, Italy

¹⁰Tor Vergata University of Rome, Via Della Ricerca Scientifica 1, 00133 Roma, Italy

¹¹Dipartimento di Fisica, Università degli Studi di Roma ‘La Sapienza’, P.le Aldo Moro 2, 00133 Roma, Italy

¹²Department of Physics, Ehime University, 2-5, Bunkyocho, Matsuyama, Ehime 790-8577, Japan

¹³Université Grenoble Alpes, CNRS, IPAG, 38000 Grenoble, France

¹⁴Astronomical Institute of the Czech Academy of Sciences, Boční II 1401/1, 14100 Praha 4, Czech Republic

¹⁵Department of Physics and Astronomy, 20014 University of Turku, Finland

¹⁶MIT Kavli Institute for Astrophysics and Space Research, Massachusetts Institute of Technology, Cambridge, MA 02139, USA

¹⁷Center for Astrophysics, Harvard & Smithsonian, Cambridge, MA 02138, USA

¹⁸Dipartimento di Fisica e Astronomia, Università degli Studi di Padova, Via Marzolo 8, 35131, Padova, Italy

¹⁹Nordita, KTH Royal Institute of Technology and Stockholm University, Hannes Alfvéns väg 12, SE-10691 Stockholm, Sweden

²⁰School of Physics and Astronomy, University of Southampton, University Road, Southampton SO17 1BJ, UK

²¹Departament de Física, EEBE, Universitat Politècnica de Catalunya, Av. Eduard Maristany 16, S-08019 Barcelona, Spain

²²Department of Physics and Astronomy, Michigan State University, East Lansing, MI 48824, USA

ABSTRACT

We present the first X-ray polarimetric measurement of the neutron star low-mass X-ray binary system AX J1745.6–2901 conducted by the Imaging X-ray Polarimetry Explorer (*IXPE*) satellite. This transient source, located within ~ 1.5 of the Galactic center, was observed serendipitously during a MAXI J1744–294 observation with a duration of 150 ks. The complex nature of the region in which AX J1745.6–2901 is located poses a challenge for studying its polarization. By performing a detailed analysis of the contamination from MAXI J1744–294 and the Galactic center diffuse emission, we find the source polarization degree $PD = 14.7\% \pm 4.0\%$ and polarization angle $PA = 122^\circ \pm 8^\circ$. The phase-resolved analysis shows increase in polarization during the eclipse phase, with $PD = 34.2\% \pm 8.7\%$, suggesting that the polarization-inducing mechanisms are of scattering nature, probably originating from disk winds.

Keywords: Accretion (14) — Neutron stars (1108) — Polarimetry (1278) — X-ray astronomy (1810)
— X-ray binary stars (1811)

1. INTRODUCTION

Neutron star low-mass X-ray binaries (NS-LMXBs) are systems in which a neutron star accretes material

from a low-mass companion star, typically via Roche-

lobe overflow and the subsequent formation of an accretion disk (D. Bhattacharya & E. P. J. van den Heuvel 1991; M. van der Klis 2006). These binaries are among the most luminous X-ray sources in the Galaxy, and their observable properties are shaped by a combination of accretion physics, magnetic field interactions, and geometrical orientation (D. Psaltis 2008; J. Neilsen & N. Degenaar 2023). NS-LMXBs can appear either as persistent emitters or as transients, depending on the long-term stability of the accretion disk (Y. Tanaka & N. Shibazaki 1996; A. R. King & H. Ritter 1998). Transient systems undergo episodic outbursts, during which the X-ray luminosity can increase by several orders of magnitude before returning to a quiescent state. These outbursts are generally understood to be the result of thermal-viscous instabilities in the accretion disk (A. R. King et al. 1996; J.-P. Lasota 2001), and offer key opportunities to study accretion physics across a wide range of mass inflow rates (C. Done et al. 2007).

Throughout an outburst, transient NS-LMXBs show complex broadband spectra: thermal X-ray emission from the disk and neutron star surface, hard X-ray components simply modeled with a power-law resulting from Comptonization by thermal electrons in the corona, and often, relativistic jets and/or winds (S. Migliari & R. P. Fender 2006; M. J. Church et al. 2006; J. Neilsen & N. Degenaar 2023). Their spectra evolve through well-defined states (G. Hasinger & M. van der Klis 1989; M. van der Klis 1994), and timing analysis often reveal coherent pulsations, quasi-periodic oscillations (QPOs), and type-I thermonuclear X-ray bursts (T. Strohmayer & L. Bildsten 2006; M. van der Klis 2006). Systems with high orbital inclination may also display eclipses and dipping behavior, providing direct constraints on the geometry of the accretion flow (N. E. White & J. H. Swank 1982; Y. Hyodo et al. 2009). These characteristics make transient NS-LMXBs powerful laboratories for studying accretion physics, boundary-layer (BL, region where the accretion disk meets the neutron star) emission, and the coupling between accretion state and outflows (N. A. Inogamov & R. A. Sunyaev 1999; R. Popham & R. Sunyaev 2001). Despite extensive spectral and timing studies, many aspects of their geometry and radiative processes remain difficult to probe, particularly those involving scattering and asymmetries in the disk structure (C. Done et al. 2007). X-ray polarimetry provides a promising new tool to directly probe these geometric and radiation characteristics by offering access to emission geometry, scattering environments, and magnetic field configurations (J. D. Schnittman & J. H. Krolik 2009; E. Churazov et al. 2017). Through model-dependent spectro-polarimetry, the polarization degree

(PD) of the BL of a few Z-sources has been measured: in the case of GX 5–1, S. Fabiani et al. (2024) identified polarization produced by the boundary layer at values $5.7\% \pm 1.4\%$ while the source was in the horizontal branch (HB) and $4.3\% \pm 2.0\%$ integrated over normal (NB) and flaring branches (FB); a PD of the BL component $\approx 4\%$ for Cygnus X-2 possibly in the normal branch was reported by R. Farinelli et al. (2023); in the case of XTE J1701–462 (M. Cocchi et al. 2023) a value of $6.0\% \pm 0.5\%$ was found for the hard blackbody component while the source was in the HB, with a drop of PD to $1.2\% \pm 0.7\%$ in the NB. Interesting results have been achieved in the Atoll sources as well. The reflection component present in the spectra of GX 9+9 (F. Ursini et al. 2023) was found to be polarized at 10%, resulting in $3 \pm 1\%$ polarization of BL. In the case of GS 1826–238, only an upper limit on PD was found at $\lesssim 1.3\%$ (F. Capitanio et al. 2023). On the other hand, A. Di Marco et al. (2023a) have found 4U 1820–303 to have the reflection component polarized at $5.3 \pm 0.2\%$.

AX J1745.6–2901 is a transient NS-LMXB located just $\sim 1'.5$ from Sgr A*, at the dynamical center of the Milky Way (Y. Maeda et al. 1996; J. A. Kennea & G. K. Skinner 1996; Y. Hyodo et al. 2009; G. Ponti et al. 2015). Its location in the densely populated and strongly absorbed Galactic Center region (M. Morris & E. Serabyn 1996; M. P. Muno et al. 2009) poses observational challenges. The nature of the compact object is confirmed by the detection of type-I X-ray bursts (Y. Maeda et al. 1996; Y. Hyodo et al. 2009). The source exhibits periodic eclipses every ~ 8.35 hours together with complex dipping behavior – signatures of a nearly edge-on disk geometry (Y. Maeda et al. 1996; Y. Hyodo et al. 2009). The estimate on the source inclination is $i \sim 70^\circ - 80^\circ$ (G. Ponti et al. 2015, 2018). Studying this source provides a valuable opportunity to probe accretion and outflow physics in a high-inclination system (Y. Hyodo et al. 2009; G. Ponti et al. 2015, 2018).

The system shows strong X-ray variability, transitioning between long, bright outbursts and deep quiescence (W. Chen et al. 1997; G. Ponti et al. 2015). Archival XMM–Newton observations reveal that the source remains in outburst roughly one-third of the time, where it alternates erratically between hard and soft spectral states, with 3–10 keV fluxes of $(1-5) \times 10^{-11} \text{ erg cm}^{-2} \text{ s}^{-1}$ in the former, and $(1-3) \times 10^{-10} \text{ erg cm}^{-2} \text{ s}^{-1}$ in the latter (G. Ponti et al. 2018). In the soft state, Fe XXV and Fe XXVI absorption lines are prominent, consistent with the presence of a highly ionized wind (G. Ponti et al. 2015; J. Neilsen & N. Degenaar 2023). These features disappear in the hard state (G. Ponti et al. 2018), but this cannot be

linked to the evolution of the outflow itself, as thermal instabilities prevent the formation of absorption lines from highly ionized elements when the plasma is illuminated by radiation with a hard spectrum (J. Frank et al. 2002; S. Bianchi et al. 2017). The absorbing gas has a large column density ($N_{\text{H}} \geq 10^{23} \text{ cm}^{-2}$) and is turbulent ($v_{\text{turb}} \geq 500 \text{ km s}^{-1}$), with small $K\alpha/K\beta$ line ratios for highly ionized iron lines further indicating large column depths (Matsunaga et al., in prep.; D. Proga & T. R. Kallman 2004; G. Ponti et al. 2015).

The soft-state spectrum is well modeled by thermal components — typically a disk blackbody and a blackbody associated with cooling radiation from the NS surface — along with interstellar dust scattering and iron emission lines (K. Mitsuda et al. 1984; K. Makishima et al. 1986; Y. Hyodo et al. 2009). A Comptonized disk, and thus traces of corona, are also found to fit the soft spectral state well (G. Ponti et al. 2018), although a thermal-Comptonization component would be weaker than the others. This makes AX J1745.6–2901 particularly interesting to verify the accretion disk polarization models (S. Chandrasekhar 1960; V. M. Loskutov & V. V. Sobolev 1982).

High-inclination LMXBs like AX J1745.6–2901 offer an especially favorable viewing angle to the system geometry for X-ray polarimetric studies, which can probe disk symmetry, constrain the orientation of reprocessing structures, and reveal the presence of scattering media such as winds or bulges (H. Krawczynski et al. 2011; S. Fabiani et al. 2014; S. Fabiani & F. Muleri 2014; E. Churazov et al. 2017; A. P. Nitindala et al. 2025). In particular, asymmetries of the disk (C. Jin et al. 2018), boundary or spreading layer, and absorbing material are expected to produce measurable polarization signals (J. D. Schnittman & J. H. Krolik 2009; R. Farinelli et al. 2024; A. Bobrikova et al. 2025). The absence of a strong Comptonized corona in AX J1745.6–2901 further enhances the interpretability of any detected polarization, making it an ideal candidate for probing the origin and structure of the component responsible for the soft-state emission (J. Neilsen & N. Degenaar 2023).

In this paper, we report on the first X-ray polarimetric observation of the transient source AX J1745.6–2901 by the Imaging X-ray Polarimetry Explorer (IXPE; M. C. Weisskopf et al. 2022; P. Soffitta et al. 2021). We present the observed energy-averaged and time-resolved polarimetric properties of the source. The data reduction is described in Section 2, and the results of data analysis and their implications for the properties of the system is presented in Section 3. We discuss the analysis and the interpretation of the data in Section 4 and finally, we summarize our findings in Section 5.

2. OBSERVATION AND DATA REDUCTION

AX J1745.6–2901 is a transient low-mass X-ray binary system that was serendipitously observed in the *IXPE* field of view during a DDT observation of MAXI J1744–294 (L. Marra et al. 2025). The observation started 2025 April 5 at 07:36:34 UTC and ended on April 8 at 02:09:33 UTC, for a total livetime of ≈ 150 ks, with OBSID: 04250301. We downloaded Level 1 and Level 2 data from the public HEASARC data archive.¹ We adjusted the timing of the event arrival relative to the solar system’s barycenter applying the `barycorr` tool from the `FTOOLS` package and performed background rejection according to A. Di Marco et al. (2023b), as AX J1745.6–2901 is a relatively low-brightness source.

We chose a circular region centered on AX J1745.6–2901 and of radius $20''$, to limit the extraction to the region in which the source of our interest is significantly brighter than the contamination from MAXI J1744–294. The source count rate is $\approx 0.22 \text{ count s}^{-1} \text{ arcmin}^{-2}$, per Detector Unit (DU). The proximity of MAXI J1744–294 and Sgr A*, at a mere $\lesssim 1.5$ from AX J1745.6–2901, makes it challenging to disentangle the source emission from the different background contributions. We could not extract an annular background region centered around AX J1745.6–2901 due to the high contamination by MAXI J1744–294, which was observed with a much larger count rate of $\approx 1.14 \text{ counts s}^{-1} \text{ arcmin}^{-2}$ in the selected region. Therefore, we examine several possibilities, as depicted in Figure 1. There we show the AX J1745.6–2901 source region marked “SRC” and our background regions marked “1”–“8”. The regions are placed as follows: we identify the pixel with the highest count rate of MAXI J1744–294 and establish it as the center of the white ring with inner and outer radii of $60''$ and $100''$, respectively. For the source region, we select a circle with a radius of $20''$ centered on AX J1745.6–2901’s position, within the white ring. We place seven evenly distributed circular regions of the same radius along the ring, noted as “1”–“7”. The last background region of choice is a semicircular annulus, marked “8”, positioned diametrically opposite the source region. We explore the effect of using each of these regions independently as a distinct background in order to assess the robustness of our conclusions.

The SAOIMAGEDS9 tool and the `xpselect` feature of the IXPEOBSSIM software (v. 31.0.1; L. Baldini et al. 2022) were consecutively used to respectively define the

¹ <https://heasarc.gsfc.nasa.gov/docs/ixpe/archive/>

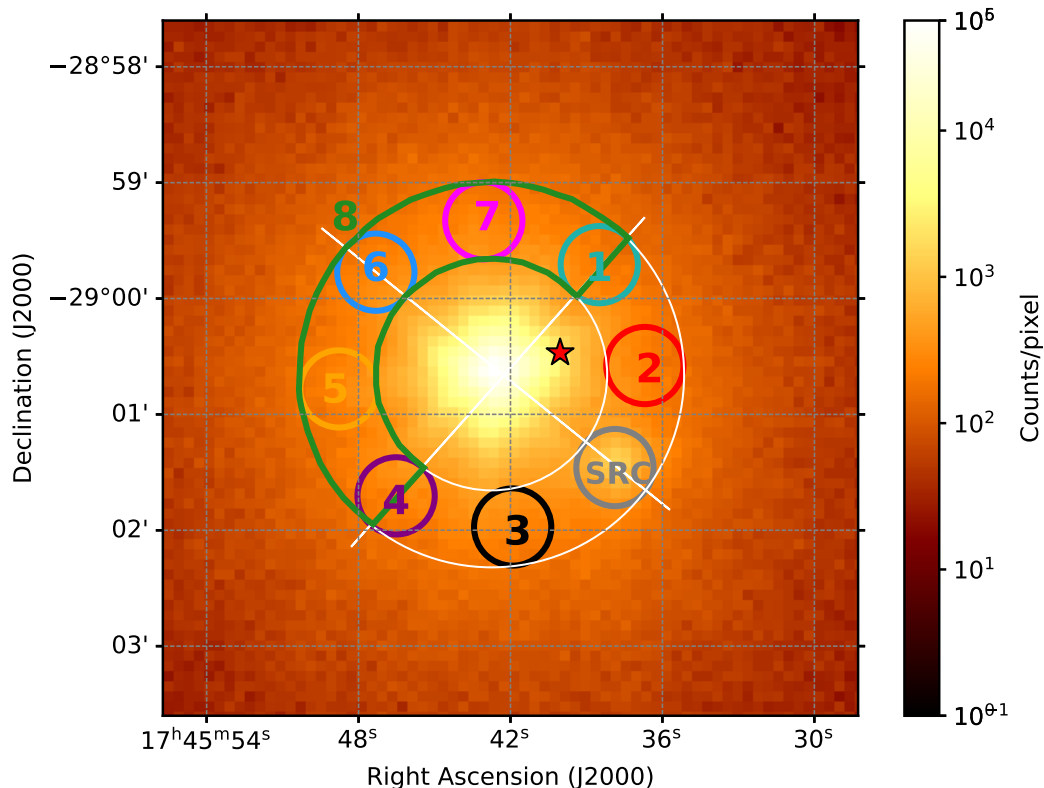


Figure 1. IXPE image of MAXI J1744–294 (bright source in the center of the FOV) and AX J1745.6–2901 (SRC) in gray. The red star marks the position of Sgr A*. The selected circular background regions are numbered 1 to 7. The dark green semicircular annulus represents the 8th region, chosen to be diametrically opposite of the source region, as highlighted by the white guidelines. The two guidelines intersect the center of MAXI J1744–294, defined as the pixel with the highest count rate.

source and background regions and to select the studied region. The `xpbin` tool within the IXPEOBSSIM package was then used to generate polarization cubes (through the `pcube` algorithm) and to create the Stokes spectra I , Q , and U . Lastly, we used the FTOOLS `ftgrouppha` task to rebin the background-subtracted Stokes spectra to require 3 counts per bin for Stokes I and 5 counts per bin for Q and U . We applied unweighted (`pcube`) and weighted (Stokes I , Q , U) analysis using the v. 20240701_v013 response matrices, which is the latest version provided with IXPEOBSSIM v 31.0.1. A model-dependent analysis was performed on the binned spectra using the HEASOFT package XSPEC software (version 12.15; K. A. Arnaud 1996). For phase-folded analysis, we extracted light curves using the FTOOLS task `xselect`, then `lcmath` to subtract background from light curves and sum the three DUs. In order to fold the light curves and obtain the orbital profile, the `efold` tool was used. Next, `xselect` was used to filter the orbital phases that correspond to eclipse and dip. Finally, `xpbin` tool from IXPEOBSSIM was applied to extract pcubes from the phase-filtered data.

3. RESULTS

3.1. Source and background polarization

To ascertain the model-independent polarization, we applied the `pcube` algorithm of IXPEOBSSIM, obtaining the energy-averaged polarization degree (PD) and polarization angle (PA) shown in Figure 2. First, we assessed the source itself (no background subtracted) and found the $PD = 8.9\% \pm 2.9\%$ and $PA = 121^\circ \pm 9^\circ$. The tentative PD (if considering two decimal places) lays above the minimum detectable polarization (MDP) value at the 99% confidence level (M. C. Weisskopf et al. 2010; T. E. Strohmayer & T. R. Kallman 2013) of 8.9%, hinting that the source could be polarized. However, this signal is likely diluted by the strong, unpolarized emission from MAXI J1744–294, for which a 3σ upper limit on the PD of 1.3% was derived by L. Marra et al. (2025). To investigate this further, we therefore examined the polarization properties of the source after subtracting different background regions individually, as illustrated in Figure 1 and explained in Section 2. We report the

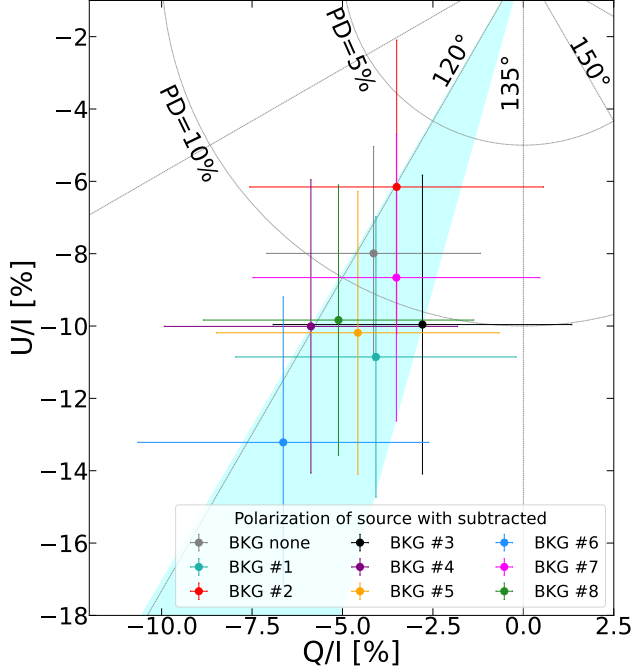


Figure 2. Normalized Stokes parameters U/I vs. Q/I of the source with different background subtractions. The gray point labeled as “BKG none” refers to the polarization of the source region without background subtraction. The values of PD and PA from the combined data of the three DUs, for each background can be read using the gray grid. The points (plotted with 1σ errors) are clustered within an angular wedge of size $\approx 10^\circ$, regardless of the background region subtracted. The clustering is represented by the cyan wedge. The gray grid represents the PD (in %) and PA (in degrees).

measured PD and PA of the source with respective MDP values (where applicable) in the left panel of Table 1.

However, to properly interpret these background-subtracted measurements, we must first verify our assumption that the background regions are unpolarized. Given the crowded nature of the Galactic Center, we cannot exclude the presence of unresolved polarized sources contained in the selected background regions.

After calculating the `pcube` of the background regions (right panel of Table 1), it is clear that only one of the background regions (“2”) appears significantly polarized, as its $PD = 15.8\% \pm 5.2\%$ is slightly above $MDP = 15.7\%$. This region is also the closest one to Sgr A*, so it could harbor some contamination. To further examine our polarization measurements independently of background subtraction effects, we tested another diagnostic: the consistency of the PA values across different background region subtractions.

Another clue hinting towards the source being polarized comes from the consistency of PA values across dif-

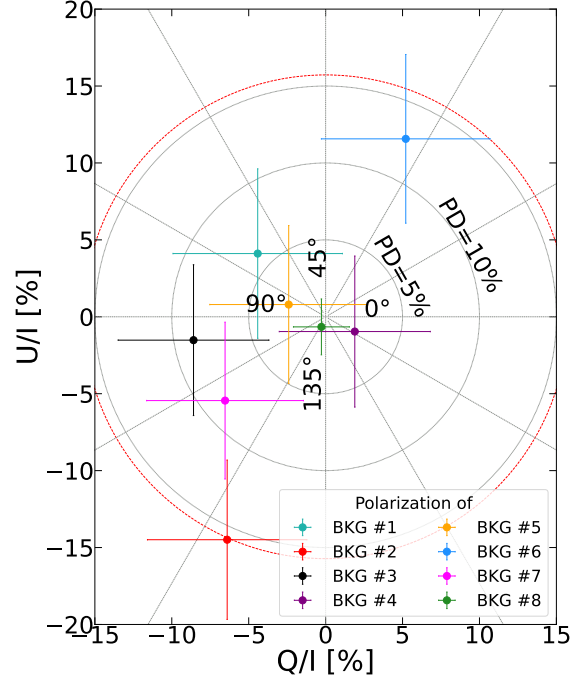


Figure 3. Normalized Stokes parameters U/I vs. Q/I of different background regions. The values of PD and PA of the sum of the three DUs, for each background, can be read using the gray grid. The only region with a PD above MDP is region “2” (in red), which is probably polarized. All other regions are well below the MDP and have scattered PA. The gray grid represents the PD (in %) and PA (in degrees). The red circle represents the MDP value for background region “2”.

ferent background subtractions. For a truly polarized source, the measured PA should remain consistent regardless of which background region is subtracted. If the PA values vary significantly between different background subtractions, it suggests the signal may be dominated by noise rather than true polarization. In Figure 2, we show the normalized Stokes parameters U/I vs. Q/I for the source after different background region subtractions. Using the secondary (gray) grid, we can also read the values of PD and PA. It is a robust sign that the PA stays consistent irrespective of the background subtracted. The dispersion of the measured PA values stays within the wedge of $\Delta PA \sim 10^\circ$. The background regions, on the contrary, show a rather “non-concentrated” distribution of PA values (Figure 3).

Considering the complexity of the Galactic Center and the fact that it is highly populated with sources, it is a difficult task to choose the “right” background region. The logical step would be to consider a region that is diametrically opposite to the source region (for symmetry reasons), and that contains the least number of AX J1745.6–2901 source counts possible (to limit self-

Subtracted BKG	PD [%]	PA [deg]	MDP [%]	Studied BKG	PD [%]	PA [deg]	MDP [%]
none	8.9 ± 2.9	121 ± 9	8.9	none	-	-	-
1	11.5 ± 3.9	unconstrained (~ 125)		1	6.0 ± 5.5	unconstrained (~ 69)	16.7
2	7.0 ± 4.1	unconstrained (~ 120)		2	15.8 ± 5.2	123 ± 9	15.7
3	10.3 ± 4.1	unconstrained (~ 127)		3	8.7 ± 4.9	unconstrained (~ 95)	14.9
4	11.5 ± 4.0	unconstrained (~ 120)		4	2.1 ± 4.9	unconstrained (~ 167)	14.9
5	11.2 ± 3.9	unconstrained (~ 123)		5	2.5 ± 5.1	unconstrained (~ 81)	15.6
6	14.7 ± 4.0	122 ± 7.8		6	12.7 ± 5.5	unconstrained (~ 33)	16.6
7	9.4 ± 4.0	unconstrained (~ 124)		7	8.5 ± 5.1	unconstrained (~ 110)	15.5
8	11.1 ± 3.7	121 ± 10		8	0.7 ± 1.8	unconstrained (~ 124)	5.5

Table 1. Left: Polarization degree and angle of AX J1745.6–2901 after subtracting various background regions shown in Figure 1 with “none” corresponding to the polarization of the source without background subtraction. MDP value is listed for the source before background subtraction. For values where the PD value is lower than $3 \times$ its uncertainty, we consider the PA unconstrained. Right: Polarization degree, angle, and MDP values of respective background regions shown in Figure 1. The reported errors correspond to 1σ . For unconstrained PA cases the most probable value is indicated.

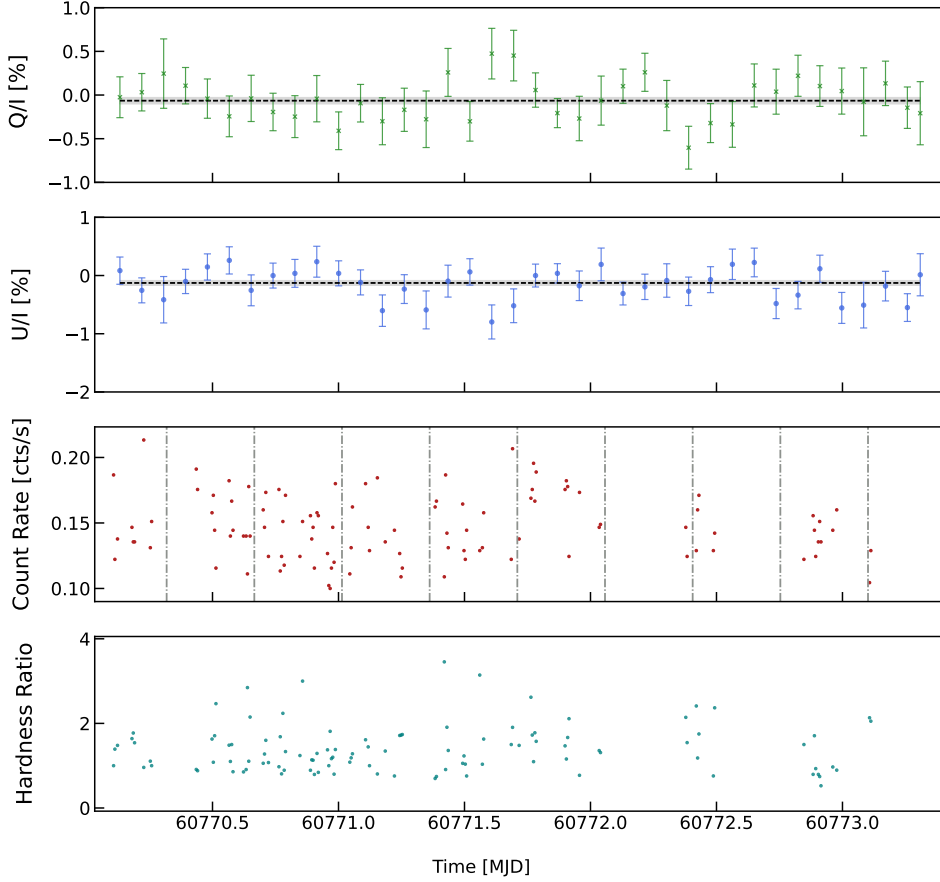


Figure 4. First and second sub-panels (respectively): normalized Stokes parameters Q/I and U/I as a function of time. The data are binned in intervals of 7.5 ks and are energy-averaged over the 2–8 keV band. The dark gray dashed line represents the constant fit, its 1σ error is represented by the shaded area. Third sub-panel from top: time evolution of count rate in the 2–8 keV band. Gray lines represent expected eclipses. Fourth sub-panel: time evolution of hardness ratio defined as a ratio between 4–8 keV and 2–4 keV count rates. The count rate and hardness ratio show data binned in intervals of 300 s. Each data point in all subplots represents the sum of the 3 DUs.

subtraction). This leaves us with only two choices: regions “6” and “8”. Since the latter spans a vast area, it poses a higher chance of including an uncontrolled effect, such as containing an unresolved source (i.e., a source that we cannot distinguish but is polarized). Part of region “8” is also in the vicinity of Sgr A*, and we cannot exclude possible contamination. Background region “6” however, satisfies both conditions of being far from Sgr A* and being in a reasonable position with respect to both MAXI J1744–294 and AX J1745.6–2901. Moreover, this region is the most logical choice to subtract possible systematic effects which impact the spatial response to polarization of photoelectric polarimeters. These are present when the extraction region is not uniformly illuminated and manifest themselves as a polarization along the image gradient (P. Soffitta et al. 2013; N. Bucciantini et al. 2023). In our case, such systematic effects would add a radial polarization directed from the central bright spot (MAXI J1744–294), with a higher PD when the gradient is steeper. Therefore, in region “6”, this effect would be the same in direction and amplitude as in the source region and then any spurious contribution to polarization which may be present would be removed in the background subtraction process. For these reasons, we will proceed with our study of AX J1745.6–2901 considering only the background region “6”² and its subtraction from the source in order to study the polarization properties of AX J1745.6–2901.

3.2. Time-dependent analysis

In this subsection, we explore the temporal evolution of both the polarimetric and spectral properties of the source, summarized in Figure 4. We plotted the normalized Stokes parameters Q/I and U/I in the first and second sub-panels, respectively. The data shown are binned in 7.5-ks intervals over the entire observation duration. The third and fourth sub-panels from top show the count rate with expected eclipses, and the hardness ratio, respectively, binned in 300 s intervals each. We analyzed the first two datasets (Stokes parameters Q/I and U/I) to test for possible time variability of the polarimetric properties of the source. The best fit we obtained was using a constant model (gray dashed lines in the figure). Q/I and U/I are two independent variables following a normal distribution (F. Kislat et al. 2015). This allows us to sum their χ^2 and degrees of freedom in order to test the null hypothesis. We obtained $\chi^2 = 73/74$ d.o.f and null hypothesis probability of 51% for the constant

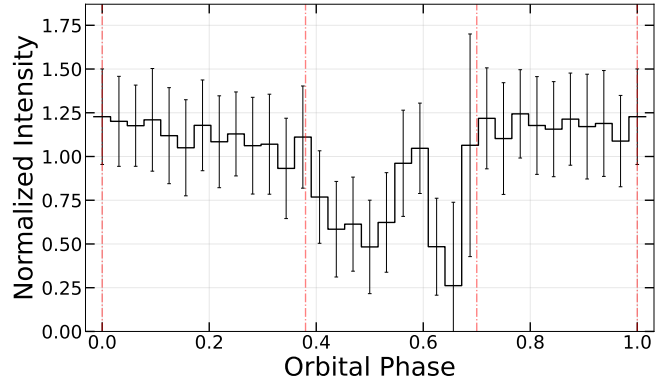


Figure 5. Phase versus normalized intensity. The plot is divided into three parts separated by red dash-dotted lines: (i) before the dip + eclipse (phase 0–0.38), (ii) dip + eclipse (phase 0.38–0.70), (iii) after the dip + eclipse (phase 0.70–1.0).

model. We conclude that the polarimetric properties stayed constant over the duration of the observation, although the high statistical uncertainties of our data limit our analysis.

3.3. Phase-resolved polarimetry

In the next step, we examine the periodic behavior of the source, focusing on the variations of the observed polarimetric properties. Using the orbital solution from G. Ponti et al. (2018), we folded the background-subtracted, summed over the three DUs, lightcurves at an arbitrary epoch into 32 bins. The dip and eclipse in the orbital profile were visually identified (Figure 5). We then extracted the source and background event files for each DU in two phase intervals, which are 0.38–0.70 (dip + eclipse) and the complementary phases. Polarization cubes were constructed from each event file. In the phase region of the dip and eclipse, we measured PD of $34.2\% \pm 8.7\%$. The corresponding PA was $127^\circ \pm 7^\circ$, which is consistent with the time-averaged result (see Figure 6). In contrast, in the phase interval outside the dip + eclipse, we found PD of $9.2 \pm 4.5\%$.

We observe a remarkably high PD during the phase with a dip and eclipse. While higher polarization during dip and/or eclipse is expected for high-inclination systems, the measured value of 34.2% is surprisingly large. This suggests that during the eclipse, the companion star obscures the central source, absorbing much of the unpolarized emission, while polarization is likely produced by scattering. Similarly, we expect that dips are related to partial obscuration by the outer regions of the disk. The scattering process is likely responsible for high polarization observed in AX J1745.6–2901. The reflecting medium is possibly either accreting disk

² While our choice of background “6” is motivated by reducing systematic effects, choosing the alternative background region “8” also provides a significant detection of polarization.

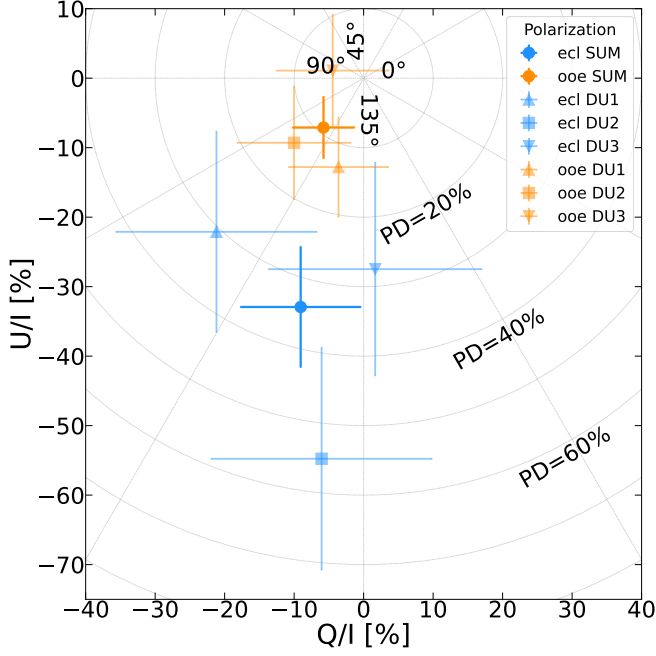


Figure 6. Normalized Stokes parameters U/I vs. Q/I of the source for different phase bins. The blue points represent the dip + eclipse (ecl), corresponding to phase 0.38 – 0.70 in Figure 5, while orange points represent the out-of-eclipse (ooe) phase, corresponding to combined regions 0 – 0.38 and 0.70 – 1. We plot a value integrated over the three DUs (labeled as SUM), as well as each DU separately (DU1, 2, and 3). The gray grid represents the PD (in %) and PA (in degrees).

winds or outflow similar to that observed in Cygnus X-3 (A. Veledina et al. 2024a,b).

3.4. Spectral properties

In our study of the source, we are also interested in disentangling the processes contributing to its X-ray emission. For this, we opt for comparing two simple models against each other: a disk blackbody versus a power law. The full model is: `constant` \times `TBabs` \times `polconst` \times `emission`, where `constant` accounts for different normalization between the three DUs of the telescope, `TBabs` is the Galactic absorption, `polconst` is a polarization model assuming constant properties in the 2–8 keV range, and `emission` is either `diskbb` (black-body accretion disk model) or `powerlaw` (photon powerlaw). The best-fit parameters are reported in Table 2 and the fits with the data residuals are shown in Figures 7–9, where we plot the contribution of each single DU and compare the two models. The two fits with `diskbb` or `powerlaw` components give $\chi^2/\text{d.o.f.} = 304/314$ (null hypothesis probability = 0.64) and $\chi^2/\text{d.o.f.} = 316/314$ (null hypothesis probability = 0.46), respectively. While in both cases we obtain statistically good results, we cannot re-

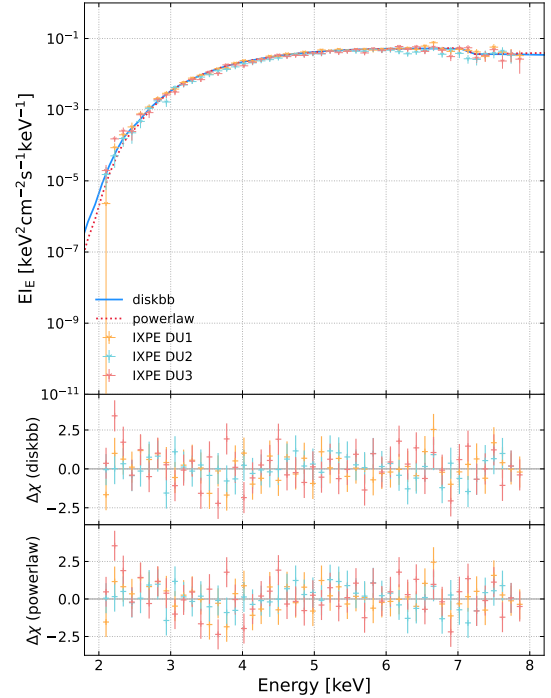


Figure 7. X-ray spectra of AX J1745.6–2901 observed with *IXPE* per each DU. Upper panel: unfolded EF_E spectra of Stokes I , comparing goodness of fit for a model with a disk blackbody (solid line) and a power law (dotted line). Lower panels: residuals of the fit $\Delta\chi$ with the disk blackbody and power-law models, respectively.

ject either model purely on the basis of the quality of fit. This can be seen from the top panel of Figure 7 where the two models overlap in the 3–7 keV energy band, and the corresponding residuals are plotted in the middle and bottom panels. While for the Stokes parameter I there is only a minor difference around 2–2.5 keV and 7.5–8 keV, for both Q and U it is practically impossible to distinguish between the two tested models, as clear from Figures 8 and 9 for Q and U , respectively. The fact that we do not manage to accurately distinguish between the two tested models is mainly due to only fitting the *IXPE* data, which are observed in a relatively narrow energy range.

Nevertheless, the spectral results we obtain are broadly consistent with the results obtained for the soft state by G. Ponti et al. (2015). Despite the statistical similarity of the two tested models, it is important to notice that the photon index of the `powerlaw` $\Gamma = 3.0$ is incompatible with the hard state (e.g., G. Ponti et al. 2015). The measured flux by *IXPE* in 2–8 keV band is $F_{2-8 \text{ keV}} = 5.1 \times 10^{-11} \text{ erg cm}^{-2} \text{ s}^{-1}$, with a hardness ratio $F_{4-8 \text{ keV}}/F_{2-4 \text{ keV}} = 8.3^{+0.1}_{-0.8}$, which corresponds to flux $F_{3-10 \text{ keV}} = 6.03 \times 10^{-11} \text{ erg cm}^{-2} \text{ s}^{-1}$ with a hardness ratio $F_{6-10 \text{ keV}}/F_{3-6 \text{ keV}} = 0.97^{+0.02}_{-0.11}$. The latter

Component	Parameter [unit]	Description	Value Fit 1	Value Fit 2
constant	C_{DU1}	Normalization	1.00	1.00
	C_{DU2}	Normalization	$0.86^{+0.04}_{-0.03}$	$0.86^{+0.04}_{-0.03}$
	C_{DU3}	Normalization	$0.91^{+0.04}_{-0.03}$	$0.91^{+0.04}_{-0.03}$
TBabs	N_H [10^{22} cm $^{-2}$]	Hydrogen column density	22.3 ± 1.2	$26.3^{+1.8}_{-1.7}$
polconst	A [%]	Polarization degree	15.4 ± 5.6	15.3 ± 5.6
	ψ [deg]	Polarization angle	120 ± 11	120 ± 11
diskbb	kT_{bb} [keV]	Inner disk radius temperature	$1.75^{+0.15}_{-0.13}$	–
	norm	Normalization	$1.51^{+0.73}_{-0.49}$	–
powerlaw	Γ	Photon index	–	$3.0^{+0.3}_{-0.2}$
	norm	Normalization	–	$0.57^{+0.36}_{-0.21}$
	$\chi^2/\text{d.o.f.}$		304/314	316/314

Table 2. Best-fit parameters of the *IXPE* spectral fitting using the model described in Section 3.4. Uncertainties are reported at 90% confidence level. The parameters in bold were frozen during the fit.

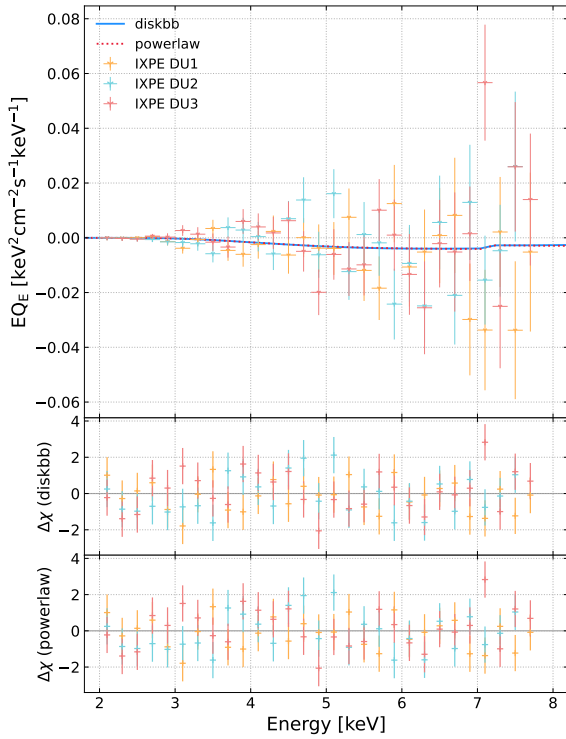


Figure 8. Same as Figure 7, but for the Stokes Q .

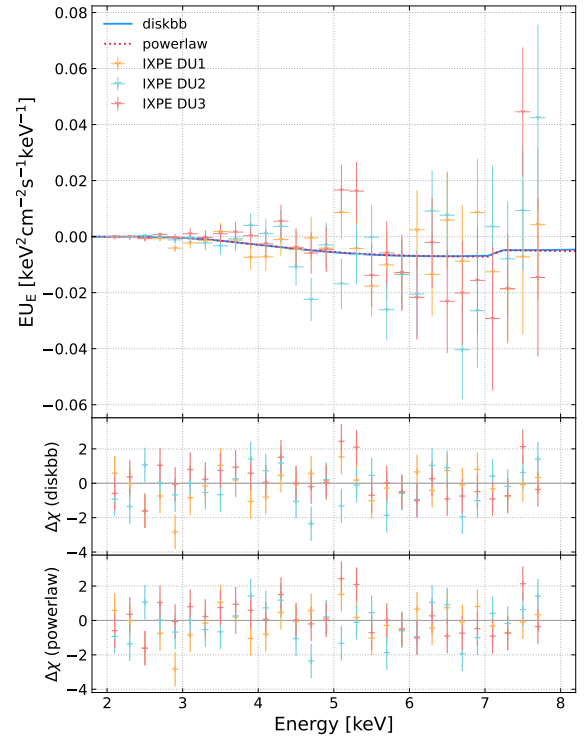


Figure 9. Same as Figure 7, but for the Stokes U .

value of the hardness ratio is consistent with the historical measurement of the source in the soft state (Fig. 3 in G. Ponti et al. 2018), while the flux would correspond to the area (in the same figure) between the hard and soft spectral states. It is possible that the source was transitioning between the two states during the *IXPE*

observation. We see from (Fig. 2 in the same paper), that the transition between the two states can take extended periods of time. Figure 10 presents the PD and PA contours from the model-dependent analysis for the *diskbb* scenario. We have created the contour plot using the `steppar` command in `xspec` with 60 steps for both

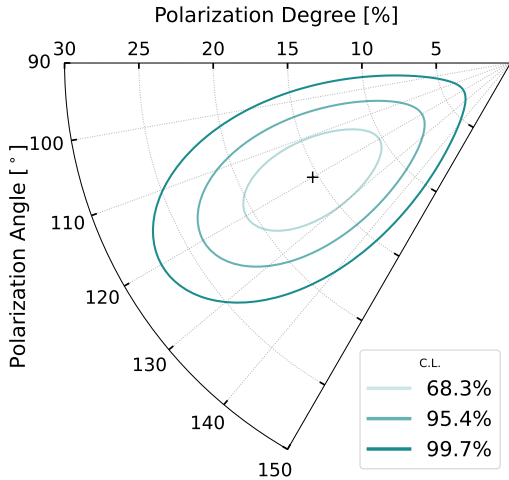


Figure 10. Polar plot of PD and PA, assuming the best spectral fit for the `diskbb` model scenario. The black “+” sign represents the best-fit value for the given model, as reported in table 2. Results shown are considering the entire *IXPE* energy band (2–8 keV). Colors are fainter with lower C.L.

PD and PA. We find the PD and PA values consistent with the `pcube` result within the error margin.

4. DISCUSSION

The serendipitous detection of AX J1745.6–2901 during the *IXPE* observation of MAXI J1744–294 represents a valuable opportunity to conduct the first X-ray polarimetric study of this neutron star LMXB system. Located within $\sim 1'5$ of the Galactic Center, AX J1745.6–2901 provides a unique laboratory for investigating polarization signatures in high-inclination accreting systems, despite the observational challenges posed by its location in this crowded and complex region. While AX J1745.6–2901 is not the first highly inclined NS-LMXB observed by *IXPE*, it presents distinctive characteristics that make it particularly interesting for polarimetric studies. Previous *IXPE* observations of the highly inclined ($i \sim 60\text{--}80^\circ$, M. Díaz Trigo et al. 2012; R. Tomaru et al. 2020) dipping source GX 13+1 revealed an average polarization degree of 2–5%, rising to $7.5\% \pm 1.7\%$ during dips (A. Bobrikova et al. 2024a,b; A. Di Marco et al. 2025; A. Di Marco 2025). More recently, observations of the eclipsing source 2S 0921–630, with an inclination of $i \sim 82^\circ$ (T. A. Ashcraft et al. 2012), measured an average PD of $8.8\% \pm 1.4\%$ (R. Tomaru et al. 2025), representing the highest polarization measured for NS-LMXBs prior to our AX J1745.6–2901 observation. The significantly higher polarization we de-

tect in AX J1745.6–2901 thus adds an important new data point to this emerging picture of polarization in high-inclination neutron star systems.

Several observational challenges significantly limit the depth of our analysis. The proximity of the much brighter MAXI J1744–294 ($\sim 1'3$ away) creates substantial difficulties in background subtraction, as conventional annular background regions cannot be utilized without severe contamination, thus requiring a completely different approach. The extremely crowded nature of the Galactic Center region further complicates the selection of appropriate background areas, forcing us to rely on carefully chosen circular regions that may not perfectly represent the local background conditions around AX J1745.6–2901. The intrinsic faintness of AX J1745.6–2901 (count rate ≈ 0.22 count s^{-1} arcmin $^{-2}$) adds to the aforementioned difficulties, resulting in relatively large statistical uncertainties that limit our ability to constrain the polarization properties with high precision.

The temporal analysis did not show any significant variations of the polarimetric properties throughout the 150 ks observation. AX J1745.6–2901 exhibits clear eclipses and dipping behavior in X-ray intensity tied to its orbital phase (G. Ponti et al. 2015, 2018). Our phase-resolved analysis reveals an increase of polarization degree from $\approx 9\%$ outside of eclipse to $\approx 34\%$ during dip and eclipse phase. This increase in polarization degree points towards scattering processes as polarization-inducing mechanisms, likely originating in disk winds.

The low signal-to-noise ratio also impacts our spectral analysis, where we find that both disk blackbody and power-law models provide statistically acceptable fits ($\chi^2/\text{d.o.f.} = 304/314$ and $316/314$, respectively) with comparable goodness-of-fit statistics. While we cannot confidently distinguish between disk blackbody and power-law emission models based on spectral fitting alone, the high photon index of our power-law fit and the broad consistency of our model parameters, flux and hardness ratio with those reported by (G. Ponti et al. 2015) for soft state observations suggest that AX J1745.6–2901 was likely in a soft spectral state during our observation. Under this soft state interpretation, the observed polarization signal can be more confidently attributed to geometrical asymmetries in the thermal emission components, such as disk inclination effects, boundary layer structure, or scattering in moderately ionized winds, rather than non-thermal processes associated with hard-state Comptonization.

The degeneracy between thermal disk emission and non-thermal power-law components is particularly problematic for understanding the accretion state and the

mechanisms responsible for the observed polarization. In thermal-dominated states, polarization might arise from scattering in the disk atmosphere (S. Chandrasekhar 1960; V. V. Sobolev 1963; V. M. Loskutov & V. V. Sobolev 1981; R. Taverna et al. 2021) or its wind (A. P. Nitindala et al. 2025), from geometrical asymmetries and relativistic effects in the boundary layer (A. Bobrikova et al. 2025), or reflection of the spreading layer emission from the accretion disk (I. I. Lapidus & R. A. Sunyaev 1985), while power-law dominated emission could indicate Comptonization processes that would produce different polarization signatures (J. Poutanen & R. Svensson 1996). Because the *IXPE* band is restricted to the narrow 2–8 keV energy interval, this degeneracy cannot be broken, limiting our ability to fully utilize the diagnostic potential of our polarimetric measurements.

The detection of a polarization signal in AX J1745.6–2901 is particularly significant given its exceptional properties. AX J1745.6–2901 is well-suited for polarimetric studies thanks to its high inclination and history of wind detection — characteristics that may enhance polarization signatures, as evidenced by recent observations of wind-bearing sources such as the black hole binaries 4U 1630–47 (A. Ratheesh et al. 2024) and IGR J17091–3624 (M. Ewing et al. 2025), which exhibited larger polarization than previously expected. Both reflection and winds have been reported for this source (G. Ponti et al. 2018), and these processes can contribute substantially to the polarimetric signal through scattering mechanisms. The high measured PD represents the first such measurement for this source and adds to the growing catalog of polarimetric observations of NS-LMXBs, with important implications for understanding highly inclined accreting systems.

5. CONCLUSIONS

We present the first X-ray polarimetric observation of the neutron star LMXB AX J1745.6–2901 using *IXPE*, serendipitously obtained during a 150 ks observation of the nearby transient MAXI J1744–294. Our main findings are:

- AX J1745.6–2901 shows evidence for X-ray polarization with $PD = 14.7\% \pm 4.0\%$ and $PA = 122^\circ \pm 8^\circ$. The consistency of the PAs across different background subtraction choices bolsters confidence in this detection (Figures 2 and 3, and Table 1).
- No significant temporal evolution of the polarimetric properties were observed throughout the 150 ks observation (Figure 4).

- The measured PD of $14.7\% \pm 4.0\%$ is exceptionally high for NS-LMXBs, making AX J1745.6–2901 the most polarized neutron star binary observed to date — significantly exceeding the $\sim 4\text{--}5\%$ typically seen in Z-sources and reaching levels previously observed only at high energies (7–8 keV). This high polarization is consistent with the known presence of both scattering and wind signatures in this source (G. Ponti et al. 2018), which can contribute substantially to the polarimetric signal through scattering processes.
- The phase-resolved analysis shows extraordinarily high PD in the dip+eclipse phase of $34.2\% \pm 8.7\%$, while the complementary phases are unpolarized. Such a high value of PD during the eclipse and dip phase strongly suggests that emission is polarized in the disk wind via scattering mechanisms.
- Spectral analysis reveals that both disk blackbody and power-law models provide equally good fits (Figures 7–9) to the data, preventing definitive identification of the dominant emission mechanism and limiting physical interpretation of the polarization signal. However, the high photon index value of the power-law component ($\Gamma = 3.0$, Table 2) is in favor of a soft spectral state of the source.

ACKNOWLEDGMENTS

The Imaging X-ray Polarimetry Explorer (*IXPE*) is a joint US and Italian mission. The US contribution is supported by the National Aeronautics and Space Administration (NASA) and led and managed by its Marshall Space Flight Center (MSFC), with industry partner Ball Aerospace (contract NNM15AA18C). The Italian contribution is supported by the Italian Space Agency (Agenzia Spaziale Italiana, ASI) through contract ASI-OHBI-2022-13-I.0, agreements ASI-INAF-2022-19-HH.0 and ASI-INFN-2017.13-H0, and its Space Science Data Center (SSDC) with agreements ASI-INAF-2022-14-HH.0 and ASI-INFN 2021-43-HH.0, and by the Istituto Nazionale di Astrofisica (INAF) and the Istituto Nazionale di Fisica Nucleare (INFN) in Italy. This research used data products provided by the *IXPE* Team (MSFC, SSDC, INAF, and INFN) and distributed with additional software tools by the High-Energy Astrophysics Science Archive Research Center (HEASARC), at NASA Goddard Space Flight Center (GSFC).

AV acknowledges support from the Academy of Finland grant 355672. Nordita is supported in part by

NordForsk. The French contribution is supported by the French Space Agency (Centre National d’Etudes Spatiales, CNES) and the Action Thématique Processus Extrême et Multimessenger of the French CNRS. JS thank GACR project 21-06825X for the support and institutional support from RVO:67985815. FC acknowledge financial support by the Istituto Nazionale di Astrofisica (INAF) grant 1.05.23.05.06: “Spin and Geometry in accreting X-ray binaries: The first multi frequency spectro-polarimetric campaign”. AT and SF acknowledge financial support by the Istituto Nazionale di Astrofisica (INAF) grant 1.05.24.02.04: “A multi frequency spectro-polarimetric campaign to explore spin and geometry in Low Mass X-ray Bina-

ries”. VEG acknowledges funding under NASA contract 80NSSC24K1403. J.Pod. acknowledges institutional support from RVO:67985815. The USRA coauthors gratefully acknowledge NASA funding through contract 80NSSC24M0035. FMV acknowledges support from the the European Union’s Horizon Europe research and innovation programme with the Marie Skłodowska-Curie (grant agreement No. 101149685). B.D.M. acknowledges support via a Ramón y Cajal Fellowship (RYC2018-025950-I), the Spanish MINECO grants PID2023-148661NB-I00, PID2022-136828NB-C44, and the AGAUR/Generalitat de Catalunya grant SGR-386/2021

REFERENCES

- Arnaud, K. A. 1996, in ASP Conf. Ser., Vol. 101, *Astronomical Data Analysis Software and Systems V*, ed. G. H. Jacoby & J. Barnes (San Francisco: Astron. Soc. Pac.), 17–20
- Ashcraft, T. A., Hynes, R. I., & Robinson, E. L. 2012, *MNRAS*, 424, 620, doi: [10.1111/j.1365-2966.2012.21241.x](https://doi.org/10.1111/j.1365-2966.2012.21241.x)
- Baldini, L., Bucciantini, N., Lalla, N. D., et al. 2022, *SoftwareX*, 19, 101194, doi: [10.1016/j.softx.2022.101194](https://doi.org/10.1016/j.softx.2022.101194)
- Bhattacharya, D., & van den Heuvel, E. P. J. 1991, *PhR*, 203, 1, doi: [10.1016/0370-1573\(91\)90064-S](https://doi.org/10.1016/0370-1573(91)90064-S)
- Bianchi, S., Ponti, G., Muñoz-Darias, T., & Petrucci, P.-O. 2017, *MNRAS*, 472, 2454, doi: [10.1093/mnras/stx2173](https://doi.org/10.1093/mnras/stx2173)
- Bobrikova, A., Di Marco, A., La Monaca, F., et al. 2024a, *A&A*, 688, A217, doi: [10.1051/0004-6361/202450207](https://doi.org/10.1051/0004-6361/202450207)
- Bobrikova, A., Poutanen, J., & Loktev, V. 2025, *A&A*, 696, A181, doi: [10.1051/0004-6361/202452358](https://doi.org/10.1051/0004-6361/202452358)
- Bobrikova, A., Forsblom, S. V., Di Marco, A., et al. 2024b, *A&A*, 688, A170, doi: [10.1051/0004-6361/202449318](https://doi.org/10.1051/0004-6361/202449318)
- Bucciantini, N., Di Lalla, N., Romani, R. W. R., et al. 2023, *A&A*, 672, A66, doi: [10.1051/0004-6361/202245744](https://doi.org/10.1051/0004-6361/202245744)
- Capitanio, F., Fabiani, S., Gnarini, A., et al. 2023, *ApJ*, 943, 129, doi: [10.3847/1538-4357/aca888](https://doi.org/10.3847/1538-4357/aca888)
- Chandrasekhar, S. 1960, *Radiative transfer* (New York: Dover)
- Chen, W., Shrader, C. R., & Livio, M. 1997, *ApJ*, 491, 312, doi: [10.1086/304921](https://doi.org/10.1086/304921)
- Churazov, E., Khabibullin, I., Ponti, G., & Sunyaev, R. 2017, *MNRAS*, 468, 165, doi: [10.1093/mnras/stx443](https://doi.org/10.1093/mnras/stx443)
- Church, M. J., Halai, G. S., & Bałucińska-Church, M. 2006, *A&A*, 460, 233, doi: [10.1051/0004-6361:20065035](https://doi.org/10.1051/0004-6361:20065035)
- Cocchi, M., Gnarini, A., Fabiani, S., et al. 2023, *A&A*, 674, L10, doi: [10.1051/0004-6361/202346275](https://doi.org/10.1051/0004-6361/202346275)
- Di Marco, A. 2025, *Astronomische Nachrichten*, 346, e20240126, doi: [10.1002/asna.20240126](https://doi.org/10.1002/asna.20240126)
- Di Marco, A., La Monaca, F., Poutanen, J., et al. 2023a, *ApJL*, 953, L22, doi: [10.3847/2041-8213/acec6e](https://doi.org/10.3847/2041-8213/acec6e)
- Di Marco, A., Soffitta, P., Costa, E., et al. 2023b, *AJ*, 165, 143, doi: [10.3847/1538-3881/acba0f](https://doi.org/10.3847/1538-3881/acba0f)
- Di Marco, A., La Monaca, F., Bobrikova, A., et al. 2025, *ApJL*, 979, L47, doi: [10.3847/2041-8213/ada7f8](https://doi.org/10.3847/2041-8213/ada7f8)
- Díaz Trigo, M., Sidoli, L., Boirin, L., & Parmar, A. N. 2012, *A&A*, 543, A50, doi: [10.1051/0004-6361/201219049](https://doi.org/10.1051/0004-6361/201219049)
- Done, C., Gierliński, M., & Kubota, A. 2007, *A&A Rv*, 15, 1, doi: [10.1007/s00159-007-0006-1](https://doi.org/10.1007/s00159-007-0006-1)
- Ewing, M., Parra, M., Mastroserio, G., et al. 2025, *MNRAS*, 541, 1774, doi: [10.1093/mnras/staf859](https://doi.org/10.1093/mnras/staf859)
- Fabiani, S., & Muleri, F. 2014, *Astronomical X-Ray Polarimetry*
- Fabiani, S., Costa, E., Del Monte, E., et al. 2014, *ApJS*, 212, 25, doi: [10.1088/0067-0049/212/2/25](https://doi.org/10.1088/0067-0049/212/2/25)
- Fabiani, S., Capitanio, F., Iaria, R., et al. 2024, *A&A*, 684, A137, doi: [10.1051/0004-6361/202347374](https://doi.org/10.1051/0004-6361/202347374)
- Farinelli, R., Waghmare, A., Ducci, L., & Santangelo, A. 2024, *A&A*, 684, A62, doi: [10.1051/0004-6361/202348915](https://doi.org/10.1051/0004-6361/202348915)
- Farinelli, R., Fabiani, S., Poutanen, J., et al. 2023, *MNRAS*, 519, 3681, doi: [10.1093/mnras/stac3726](https://doi.org/10.1093/mnras/stac3726)
- Frank, J., King, A., & Raine, D. J. 2002, *Accretion Power in Astrophysics* (Cambridge: Cambridge University Press)
- Hasinger, G., & van der Klis, M. 1989, *A&A*, 225, 79
- Hyodo, Y., Ueda, Y., Yuasa, T., et al. 2009, *PASJ*, 61, S99, doi: [10.1093/pasj/61.sp1.S99](https://doi.org/10.1093/pasj/61.sp1.S99)
- Inogamov, N. A., & Sunyaev, R. A. 1999, *Astronomy Letters*, 25, 269, doi: [10.48550/arXiv.astro-ph/9904333](https://doi.org/10.48550/arXiv.astro-ph/9904333)
- Jin, C., Ponti, G., Haberl, F., Smith, R., & Valencic, L. 2018, *MNRAS*, 477, 3480, doi: [10.1093/mnras/sty869](https://doi.org/10.1093/mnras/sty869)
- Kennea, J. A., & Skinner, G. K. 1996, *PASJ*, 48, L117, doi: [10.1093/pasj/48.6.L117](https://doi.org/10.1093/pasj/48.6.L117)

- King, A. R., Kolb, U., & Burderi, L. 1996, *ApJL*, 464, L127, doi: [10.1086/310105](https://doi.org/10.1086/310105)
- King, A. R., & Ritter, H. 1998, *MNRAS*, 293, L42, doi: [10.1046/j.1365-8711.1998.01295.x](https://doi.org/10.1046/j.1365-8711.1998.01295.x)
- Kislat, F., Clark, B., Beilicke, M., & Krawczynski, H. 2015, *Astroparticle Physics*, 68, 45, doi: [10.1016/j.astropartphys.2015.02.007](https://doi.org/10.1016/j.astropartphys.2015.02.007)
- Krawczynski, H., Garson, A., Guo, Q., et al. 2011, *Astroparticle Physics*, 34, 550, doi: [10.1016/j.astropartphys.2010.12.001](https://doi.org/10.1016/j.astropartphys.2010.12.001)
- Lapidus, I. I., & Sunyaev, R. A. 1985, *MNRAS*, 217, 291, doi: [10.1093/mnras/217.2.291](https://doi.org/10.1093/mnras/217.2.291)
- Lasota, J.-P. 2001, *NewAR*, 45, 449, doi: [10.1016/S1387-6473\(01\)00112-9](https://doi.org/10.1016/S1387-6473(01)00112-9)
- Loskutov, V. M., & Sobolev, V. V. 1981, *Astrofizika*, 17, 97
- Loskutov, V. M., & Sobolev, V. V. 1982, *Astrophysics*, 18, 51, doi: [10.1007/BF01004467](https://doi.org/10.1007/BF01004467)
- Maeda, Y., Koyama, K., Sakano, M., Takeshima, T., & Yamauchi, S. 1996, *PASJ*, 48, 417, doi: [10.1093/pasj/48.3.417](https://doi.org/10.1093/pasj/48.3.417)
- Makishima, K., Maejima, Y., Mitsuda, K., et al. 1986, *ApJ*, 308, 635, doi: [10.1086/164534](https://doi.org/10.1086/164534)
- Marra, L., Mikušincová, R., Vincentelli, F. M., et al. 2025, arXiv e-prints, arXiv:2506.17050, doi: [10.48550/arXiv.2506.17050](https://doi.org/10.48550/arXiv.2506.17050)
- Migliari, S., & Fender, R. P. 2006, *MNRAS*, 366, 79, doi: [10.1111/j.1365-2966.2005.09777.x](https://doi.org/10.1111/j.1365-2966.2005.09777.x)
- Mitsuda, K., Inoue, H., Koyama, K., et al. 1984, *PASJ*, 36, 741
- Morris, M., & Serabyn, E. 1996, *ARA&A*, 34, 645, doi: [10.1146/annurev.astro.34.1.645](https://doi.org/10.1146/annurev.astro.34.1.645)
- Muno, M. P., Bauer, F. E., Baganoff, F. K., et al. 2009, *ApJS*, 181, 110, doi: [10.1088/0067-0049/181/1/110](https://doi.org/10.1088/0067-0049/181/1/110)
- Neilsen, J., & Degenaar, N. 2023, in *High-Resolution X-Ray Spectroscopy: Instrumentation, Data Analysis, and Science*, ed. C. Bambi & J. Jiang, Springer Series in Astrophysics and Cosmology (Singapore: Springer Nature Singapore), 291–344, doi: [10.1007/978-981-99-4409-5_11](https://doi.org/10.1007/978-981-99-4409-5_11)
- Nitindala, A. P., Veledina, A., & Poutanen, J. 2025, *A&A*, 694, A230, doi: [10.1051/0004-6361/202453188](https://doi.org/10.1051/0004-6361/202453188)
- Ponti, G., Bianchi, S., Muñoz-Darias, T., et al. 2015, *MNRAS*, 446, 1536, doi: [10.1093/mnras/stu1853](https://doi.org/10.1093/mnras/stu1853)
- Ponti, G., Bianchi, S., Muñoz-Darias, T., et al. 2018, *MNRAS*, 473, 2304, doi: [10.1093/mnras/stx2425](https://doi.org/10.1093/mnras/stx2425)
- Popham, R., & Sunyaev, R. 2001, *ApJ*, 547, 355, doi: [10.1086/318336](https://doi.org/10.1086/318336)
- Poutanen, J., & Svensson, R. 1996, *ApJ*, 470, 249, doi: [10.1086/177865](https://doi.org/10.1086/177865)
- Proga, D., & Kallman, T. R. 2004, *ApJ*, 616, 688, doi: [10.1086/425117](https://doi.org/10.1086/425117)
- Psaltis, D. 2008, *Living Reviews in Relativity*, 11, 9, doi: [10.12942/lrr-2008-9](https://doi.org/10.12942/lrr-2008-9)
- Ratheesh, A., Dovčiak, M., Krawczynski, H., et al. 2024, *ApJ*, 964, 77, doi: [10.3847/1538-4357/ad226e](https://doi.org/10.3847/1538-4357/ad226e)
- Schnittman, J. D., & Krolik, J. H. 2009, *ApJ*, 701, 1175, doi: [10.1088/0004-637X/701/2/1175](https://doi.org/10.1088/0004-637X/701/2/1175)
- Sobolev, V. V. 1963, *A treatise on radiative transfer* (Princeton: Van Nostrand)
- Soffitta, P., Muleri, F., Fabiani, S., et al. 2013, *Nuclear Instruments and Methods in Physics Research A*, 700, 99, doi: [10.1016/j.nima.2012.09.055](https://doi.org/10.1016/j.nima.2012.09.055)
- Soffitta, P., Baldini, L., Bellazzini, R., et al. 2021, *AJ*, 162, 208, doi: [10.3847/1538-3881/ac19b0](https://doi.org/10.3847/1538-3881/ac19b0)
- Strohmayer, T., & Bildsten, L. 2006, in *Compact stellar X-ray sources*, ed. W. H. G. Lewin & M. van der Klis (Cambridge: Cambridge University Press), 113–156
- Strohmayer, T. E., & Kallman, T. R. 2013, *ApJ*, 773, 103, doi: [10.1088/0004-637X/773/2/103](https://doi.org/10.1088/0004-637X/773/2/103)
- Tanaka, Y., & Shibazaki, N. 1996, *ARA&A*, 34, 607, doi: [10.1146/annurev.astro.34.1.607](https://doi.org/10.1146/annurev.astro.34.1.607)
- Taverna, R., Marra, L., Bianchi, S., et al. 2021, *MNRAS*, 501, 3393, doi: [10.1093/mnras/staa3859](https://doi.org/10.1093/mnras/staa3859)
- Tomaru, R., Done, C., & Odaka, H. 2025, arXiv e-prints, arXiv:2509.26147, doi: [10.48550/arXiv.2509.26147](https://doi.org/10.48550/arXiv.2509.26147)
- Tomaru, R., Done, C., Ohsuga, K., Odaka, H., & Takahashi, T. 2020, *MNRAS*, 497, 4970, doi: [10.1093/mnras/staa2254](https://doi.org/10.1093/mnras/staa2254)
- Ursini, F., Farinelli, R., Gnarini, A., et al. 2023, *A&A*, 676, A20, doi: [10.1051/0004-6361/202346541](https://doi.org/10.1051/0004-6361/202346541)
- van der Klis, M. 1994, *A&A*, 283, 469
- van der Klis, M. 2006, in *Compact stellar X-ray sources*, ed. W. H. G. Lewin & M. van der Klis (Cambridge: Cambridge University Press), 39–112
- Veledina, A., Muleri, F., Poutanen, J., et al. 2024a, *Nature Astronomy*, 8, 1031, doi: [10.1038/s41550-024-02294-9](https://doi.org/10.1038/s41550-024-02294-9)
- Veledina, A., Poutanen, J., Bocharova, A., et al. 2024b, *A&A*, 688, L27, doi: [10.1051/0004-6361/202451356](https://doi.org/10.1051/0004-6361/202451356)
- Weisskopf, M. C., Elsner, R. F., & O’Dell, S. L. 2010, in *Proc. SPIE, Vol. 7732, Space Telescopes and Instrumentation 2010: Ultraviolet to Gamma Ray*, ed. M. Arnaud, S. S. Murray, & T. Takahashi, 77320E, doi: [10.1117/12.857357](https://doi.org/10.1117/12.857357)
- Weisskopf, M. C., Soffitta, P., Baldini, L., et al. 2022, *JATIS*, 8, 026002, doi: [10.1117/1.JATIS.8.2.026002](https://doi.org/10.1117/1.JATIS.8.2.026002)
- White, N. E., & Swank, J. H. 1982, *ApJL*, 253, L61, doi: [10.1086/183737](https://doi.org/10.1086/183737)